Supporting information

WO_x/ZrO_x functionalised periodic mesoporous organosilicas as water-tolerant catalysts for carboxylic acid esterification

Vannia C. dos Santos-Durndell,[a+] Lee J. Durndell,[a+*] Mark A. Isaacs,[b,c] Adam F. Lee[d*] and Karen Wilson[d*]

[a]School of Geography, Earth and Environmental Sciences, Plymouth University, Plymouth, PL4 8AA, UK.

[b]Department of Chemistry, University College London, London, WC1E 6BT, UK.

[c]HarwellXPS, Research Complex at Harwell, Rutherford Appleton Laboratory, Didcot, Oxfordshire, OX11 0DE, UK.

[d]Centre for Advanced Materials and Industrial Chemistry (CAMIC), RMIT University, Melbourne VIC 3000, Australia.

[+] *These authors contributed equally to this work*

Corresponding authors: lee.durndell@plymouth.ac.uk; adamfraserlee@gmail.com; and karen.wilson2@rmit.edu.au

Experimental

Support synthesis

SBA-15 and PMO analogues containing phenyl bridged siloxane units derived from BTSB (1,4-bis(triethoxysilyl)benzene) were prepared adapting the protocol of Sánchez-Vázquez et al.[1] Briefly, 3 g Pluronic P123 triblock copolymer was dissolved in 96 cm^3 water and 1 cm^3 HCl under stirring for 24 h at 40 °C. The appropriate ratio of TEOS and BTSB precursors (to vary the proportion of Si atoms derived from TEOS versus BTSB to be between 25% and 100%) were subsequently added to the surfactant solution, which was stirred at 40 °C for a further 72 h. The mixture was then aged at 130 °C for 24 h and the resulting solid product filtered, washed three times with deionised water and dried at room temperature. Residual P123 template was extracted via two cycles of a 24 h reflux with EtOH/1 M HCl solution, then filtered and dried yielding the final powdered SBA-15 and PMO silica supports. PMO(25%) corresponds to a TEOS:BTSB molar ratio of 6:1; PMO(50%) corresponds to a molar ratio of 2:1, and PMO(100%) corresponds to no TEOS and only BTSB added. Note the overall Si/P123 molar ratio was constant in all cases at 60:1.

Tungsten and zirconia incorporation

Tungsten and zirconia were incorporated onto the PMO following a co-grafting method using tungsten chloride and zirconium propoxide as precursors adapting the protocols of Morales et al[2] and dos Santos et al.[3] Briefly 3 g PMO was dried at 100 °C for 4 h and added to 17.54 g of 70 vol% zirconium(IV) isopropoxide in propan-1-ol, 1.01 g WCl_6 (in 20 mL ethanol) and 60 mL anhydrous hexane. The mixture was refluxed at 69 °C overnight, and then filtered and washed with hexane to remove any unreacted precursor. The resulting solid was rehydrated with 60 mL deionised H_2O at room temperature under stirring for 4 h, filtered, washed with deionised H_2O and ethanol and dried at 100 °C overnight to yield the final WO_x/ZrO_x/PMO material.

Support and catalyst characterisation

Wide angle XRD patterns were recorded on a Bruker D8 Advance diffractometer with a Cu K_α (1.54 Å) source calibrated against a Si standard, between 2θ = 20-90 °, with a step size of 0.02°. Low angle XRD patterns were recorded for 2θ = 0.2-8.0 ° with a step size of 0.02 °. Nitrogen porosimetry was undertaken on a Quantachrome Nova 2000e porosimeter using NovaWin version 11 analysis software. Samples were degassed at 120 °C for 2 h before nitrogen physisorption. Adsorption/desorption isotherms were recorded for parent and impregnated silicas, with BET surface areas calculated over the relative pressure range 0.01-0.2. Pore diameters and volumes were calculated by applying the NLDFT method to desorption isotherms for relative pressures >0.35. Bulk tungsten and zirconium loadings were calculated using XRF analysis on a Bruker S8. DRIFTS measurements were conducted using a Thermo Scientific Nicolet environmental cell and smart collector accessory on a Thermo Scientific Nicolet iS50 FT-IR Spectrometer with MCT detector. Ex-situ pyridine adsorption studies were made by wetting the samples with pyridine. Excess pyridine was removed overnight in vacuo at 80 °C, with subsequent *in vacuo* analysis by DRIFTS. Acid site loadings were measured by NH_3 pulse chemisorption using a Quantachrome ChemBET 3000 instrument interfaced to an MKS Minilab mass spectrometer (MS). Samples were degassed at 120 °C overnight under helium, before NH_3 pulse titration at 100 °C. Acid strength

was examined by propylamine adsorption and subsequent TGA-mass spectrometry (MS) analysis. Catalysts were wetted with propylamine, with excess physisorbed propylamine removed in vacuo at room temperature prior to temperature programmed desorption on a Mettler Toledo TGA/DSC 2 STARe System equipped with a Pfeiffer Vacuum ThermoStarTM GSD 301 T3 mass spectrometer. Evolution of reactively-formed propene (m/z=41 amu) evidenced acid catalysed propylamine decomposition (by the Hofmann rearrangement), with lower temperature desorption indicative of stronger acid sites. Carbon content was verified using CHNS analysis via a Thermo Scientific Flash 2000 CHNS-O analyser. XPS was performed on a Kratos Axis HSi X-ray photoelectron spectrometer fitted with a charge neutraliser and magnetic focusing lens employing Al K_α monochromated radiation (1486.7 eV). Spectral fitting was performed using CasaXPS version 2.3.14, with binding energies corrected to the C 1s peak at 284.6 eV. W 4f and Zr 4p XP spectra were fitted using an asymmetric lineshape. High-resolution high-angle annular dark-field STEM images were obtained on an aberration-corrected JEOL 2100-F microscope operated at 200 kV, with image analysis using ImageJ v1.41 software. Samples were dispersed in methanol and drop cast on 200-mesh carbon-coated copper grids and dried under ambient conditions. Solid-state NMR spectra were obtained at the EPSRC UK National Solid-state NMR Service at Durham University. Silicon nuclei environments were characterized by single pulse solid state ^{29}Si magic-angle spinning (MAS)-NMR experiments at a magnetic field strength of 11.7 T on a high-resolution Bruker Avance III HD NMR spectrometer at room temperature operating, at a frequency of 79.435 MHz. Resultant spectra were recorded using a 4.0 μs π/2 pulse, a recycle delay of 30s, and 1000 transients. Proton nuclei environments were recorded under similar conditions at a frequency of approx. 400.17 MHz.

Catalytic reactions

Batch esterification reactions were performed using a Radleys Carousel reactor station at atmospheric pressure. 300 mmol methanol, 10 mmol propanoic (C_3), levulinic (C_5), hexanoic (C_6), octanoic (C_8) decanoic acid (C_{10}) or palmitic (C_{16}) acid; and 0.5 mmol dihexyl ether (as an internal standard) were added to a sealed glass reactor, containing 0.025 g catalyst, at 60 °C, stirring at 800 rpm. Aliquots were withdrawn periodically from the reaction mixture and analysed by off-line GC after dilution with methanol using a Shimadzu GC-2010 Plus system with an FID and BP50 30 m x 0.32 mm x 0.25 μm capillary column.

GC injections were performed in triplicate, with average values reported. Conversion was calculated from **Equation S1**, where n_t is the number of mmol reactant at time t, and n_0 the initial mmol acid. Errors in acid conversion were ±3 %. Turnover Frequencies (TOFs) were calculated by normalisation of initial rates derived from the linear portion of reaction profiles (during the first hour) to the acid site loadings obtained from NH_3 pulse chemisorption. Water addition experiments were performed with addition of 5 mmol deionised water.

$$\% \text{ Conversion} = [(n_0 - n_t) / (n_0)] \times 100 \qquad \textbf{Equation S1}$$

$$\text{TOF} = \text{mmol}_{\text{acid}} \text{ converted} . h^{-1} / \text{mmol}_{\text{surfaceacidsites}} \qquad \textbf{Equation S2}$$

Support and catalyst characterisation

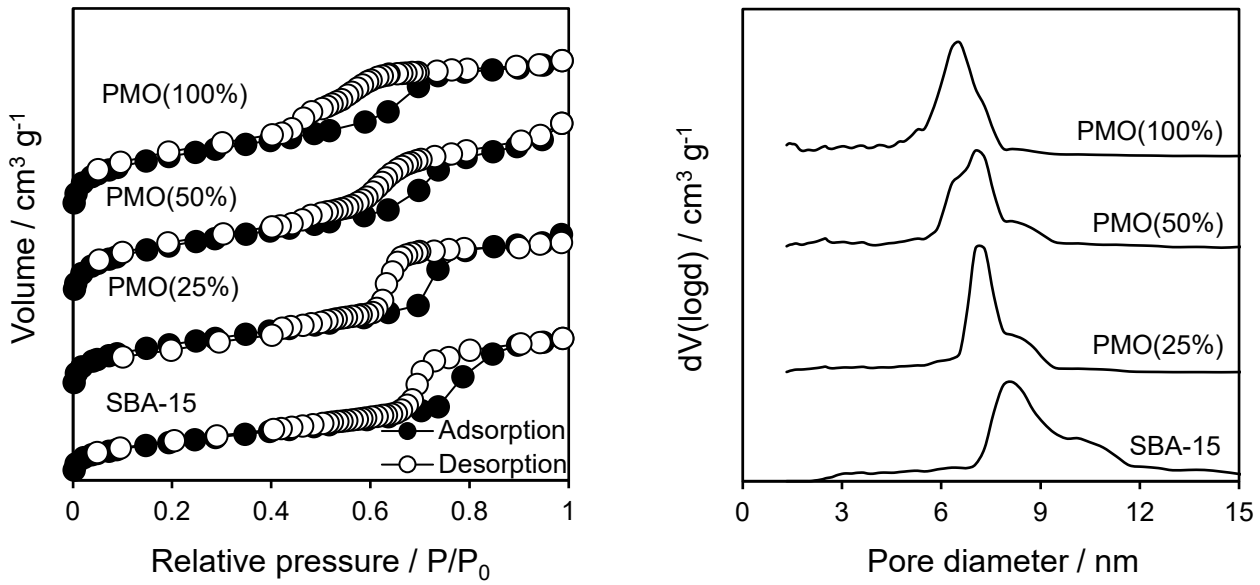

Figure S1. (*left*) N_2 adsorption-desorption isotherms, and (*right*) NLDFT pore size distributions of the parent SBA-15 and PMOs. Offset for clarity.

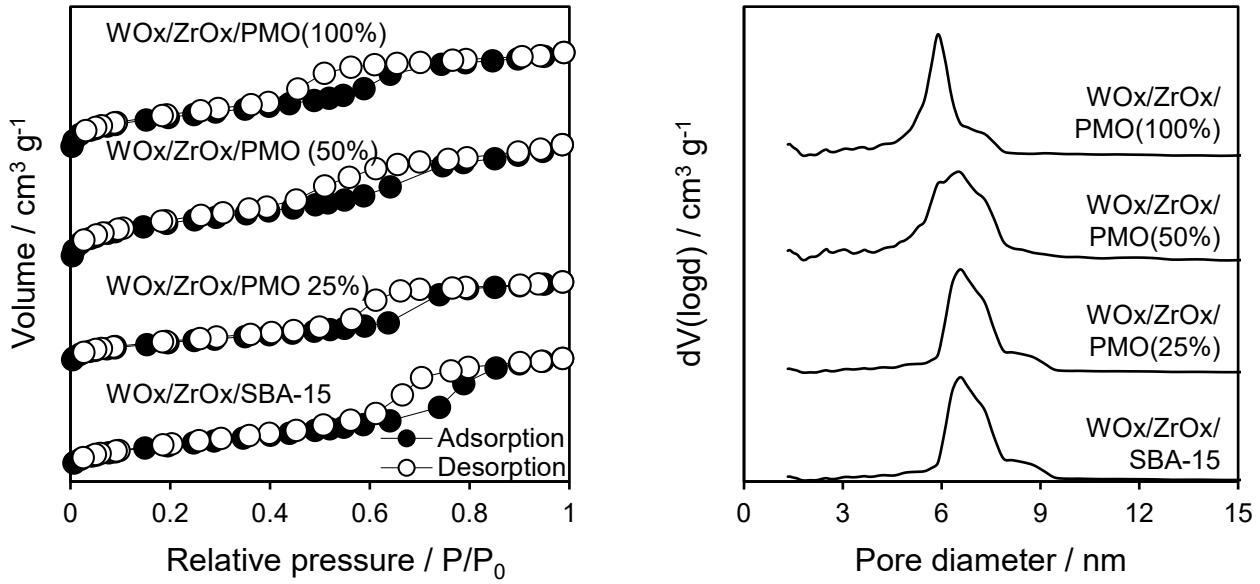

Figure S2. (*left*) N_2 adsorption-desorption isotherms, and (*right*) NLDFT pore size distributions of WO_x/ZrO_x impregnated SBA-15 and PMOs. Offset for clarity.

Table S1. Comparison of support pore diameters determined by porosimetry and microscopy.

Support	**NLDFT pore diameter / nm**	**HRTEM pore diameter / nm**
SBA-15	8.2	6.6 ± 0.34
PMO(25%)	7.0	5.7 ± 0.49
PMO(50%)	6.8	5.3 ± 0.50
PMO(100%)	6.6	4.7 ± 0.46

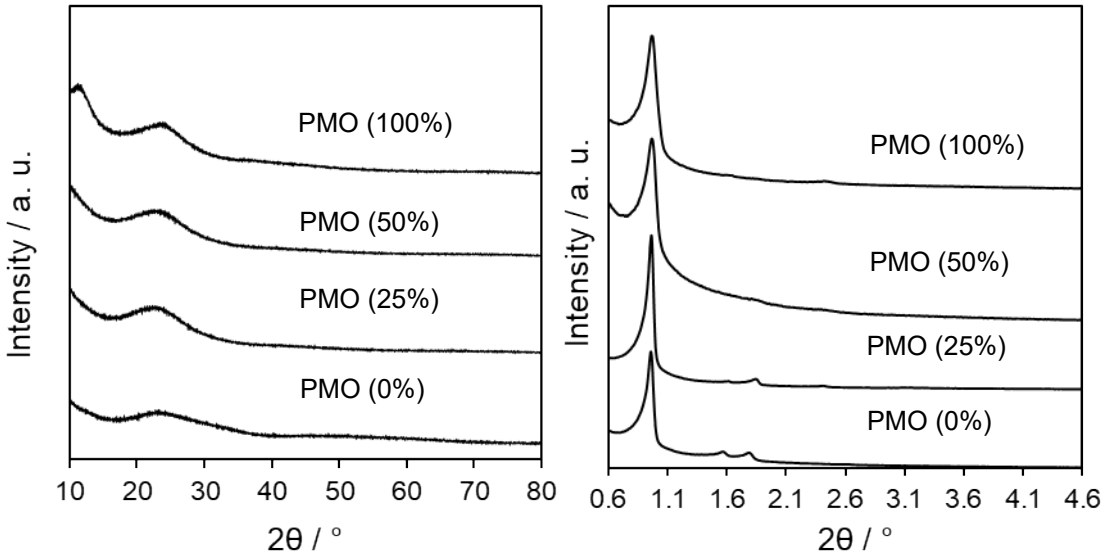

Figure S3. (*left*) Wide angle and (*right*) low angle XRD patterns of the parent SBA-15 and PMOs. Offset for clarity.

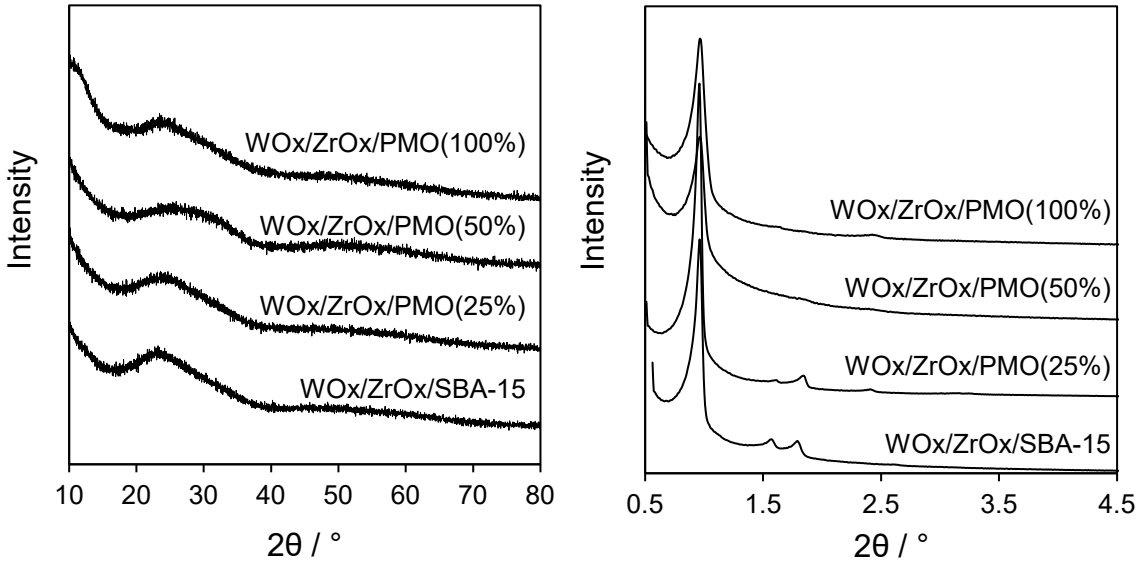

Figure S4. (*left*) Wide angle and (*right*) low angle XRD patterns of the WO_x/ZrO_x impregnated periodic mesoporous organosilica supports. Offset for clarity.

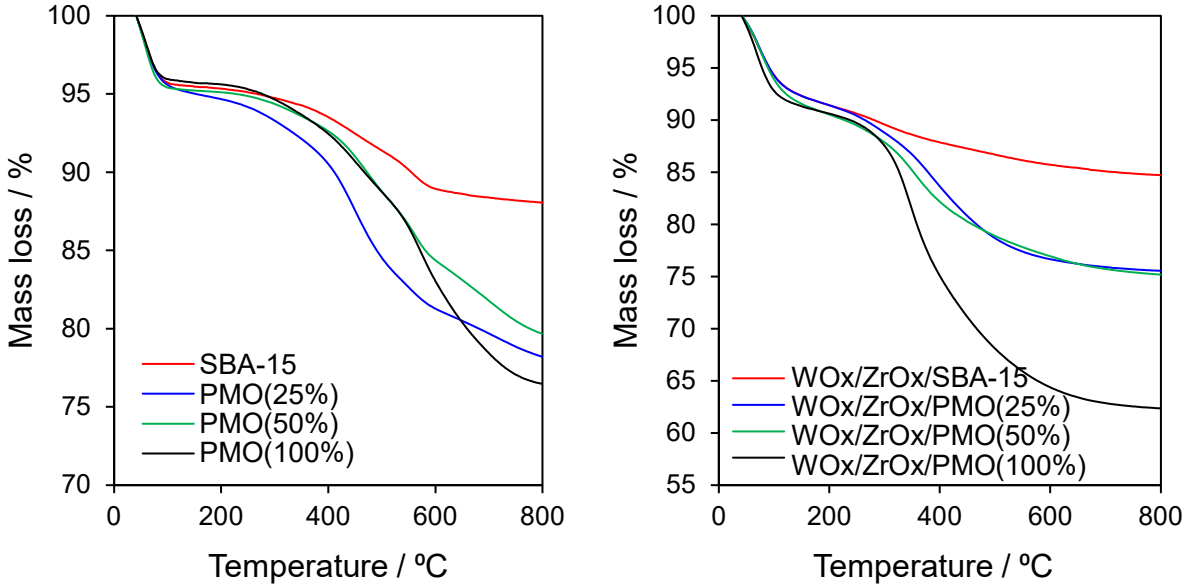

Figure S5. Thermogravimetric analysis (TGA) of (*left*) parent SBA-15 and PMOs, and (*right*) WO_x/ZrO_x impregnated SBA-15 and PMOs.

Table S2. Chemical analysis of WO_x/ZrO_x impregnated SBA-15 and PMOs.

Sample	Bulk Cl[a] / wt%	Bulk W[a] / wt%	Surface W[b] / wt%	Bulk Zr[a] / wt%	Surface Zr[b] / wt%	Bulk W:Zr mass ratio[a]	Surface W:Zr mass ratio[b]	H^+ [c] / mmol.g^{-1}
WOx/ZrOx/SBA-15	-	2.0	2.0	27.9	26.2	0.07	0.08	1.05
WOx/ZrOx/PMO(25%)	-	1.6	1.7	21.9	20.0	0.07	0.08	0.68
WOx/ZrOx/PMO(50%)	-	1.8	1.6	23.2	19.4	0.08	0.08	0.63
WOx/ZrOx/PMO(100%)	-	1.8	1.8	26.0	29.2	0.07	0.06	0.5

[a]ICP-MS. [b]XPS. [c]Propylamine TPD.

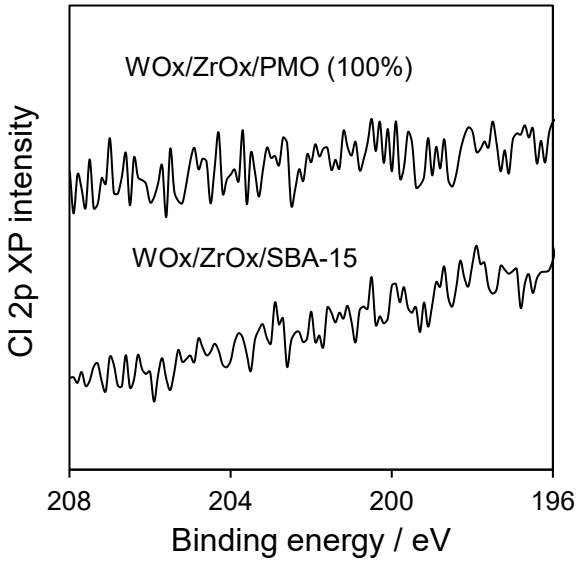

Figure S6. High-resolution Cl 2p XP spectra on WO_x/ZrO_x impregnated SBA-15 and PMO(100%) confirming the absence of surface chlorine. Offset for clarity.

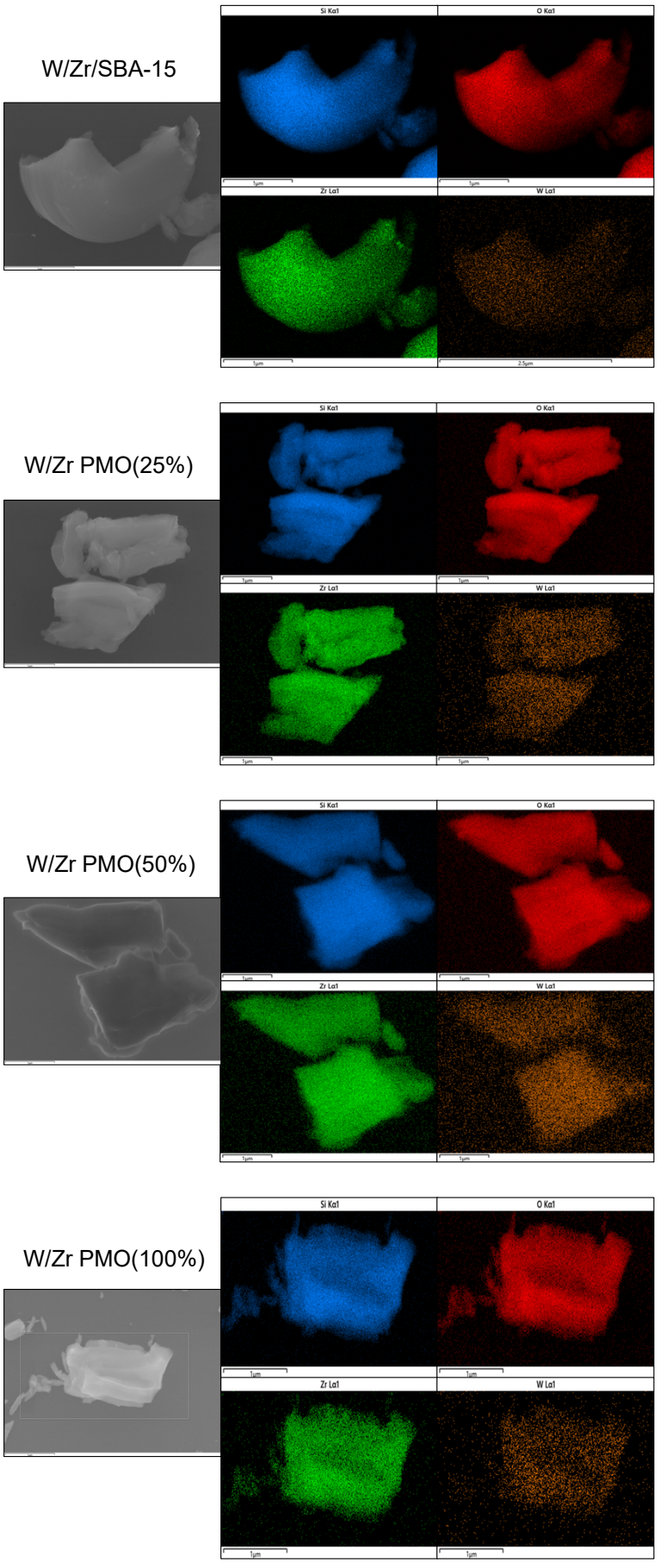

Figure S7. SEM images and corresponding EDX elemental maps (Si - blue; O - red; Zr – green; W - orange) of WO_x/ZrO_x impregnated SBA-15 and PMOs.

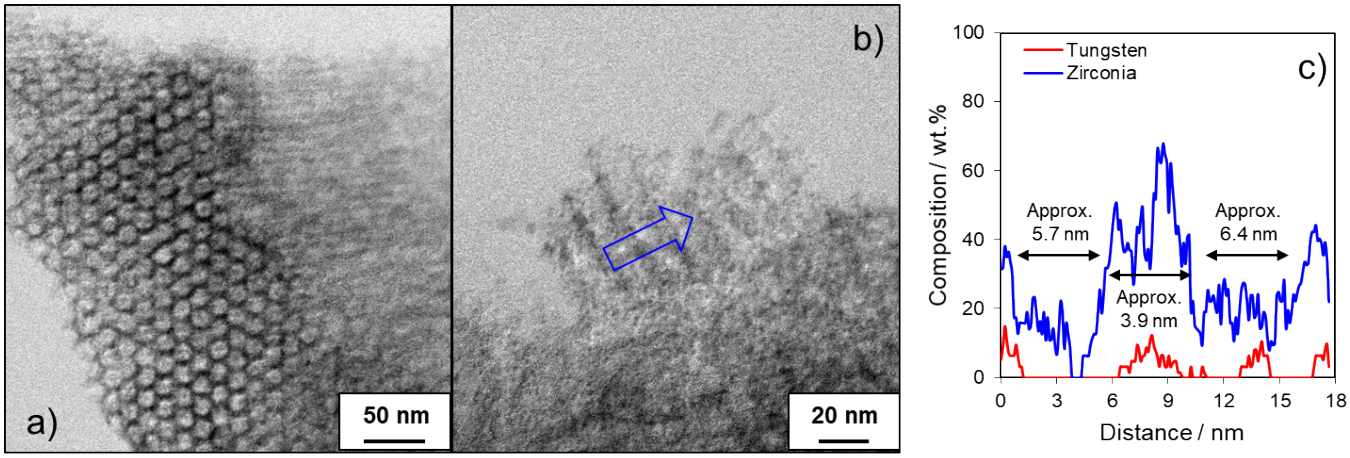

Figure S8. Representative HRTEM bright field images of WO_X/ZrOx/SBA-15, a) and b); and c) representative elemental line scans confirming the successful co-impregnation of W and Zr species into the support mesopore network.

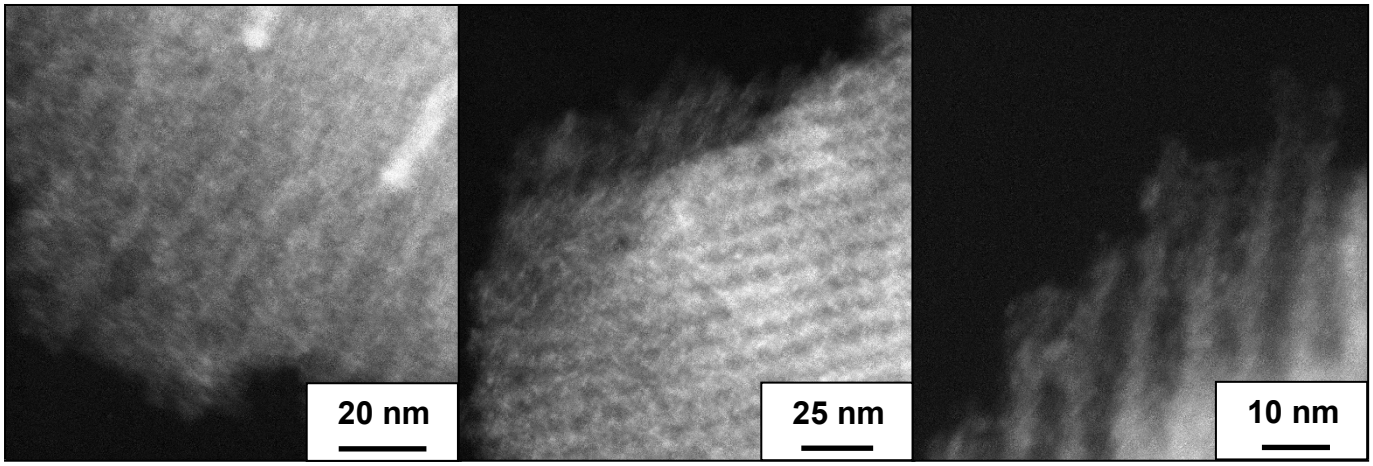

Figure S9. Representative HRTEM dark field images of WO_X/ZrOx/PMO(25%).

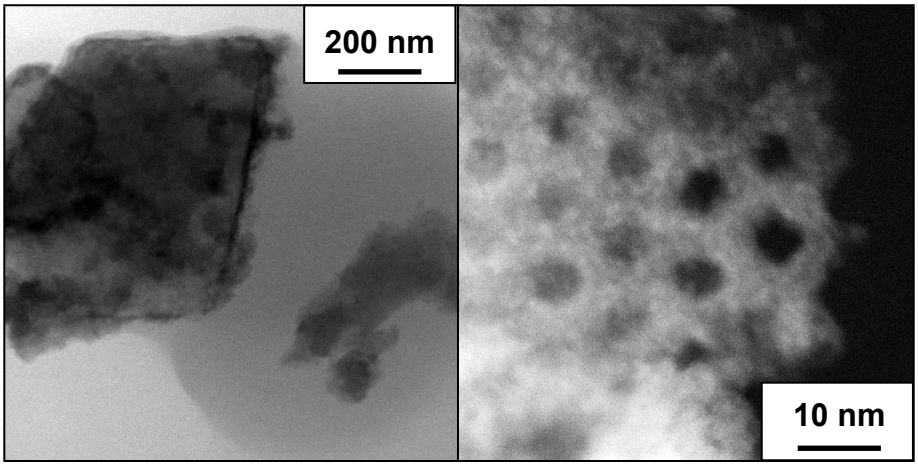

Figure S10. Representative HRTEM dark and bright field images of WO_X/ZrO_x/PMO (50%).

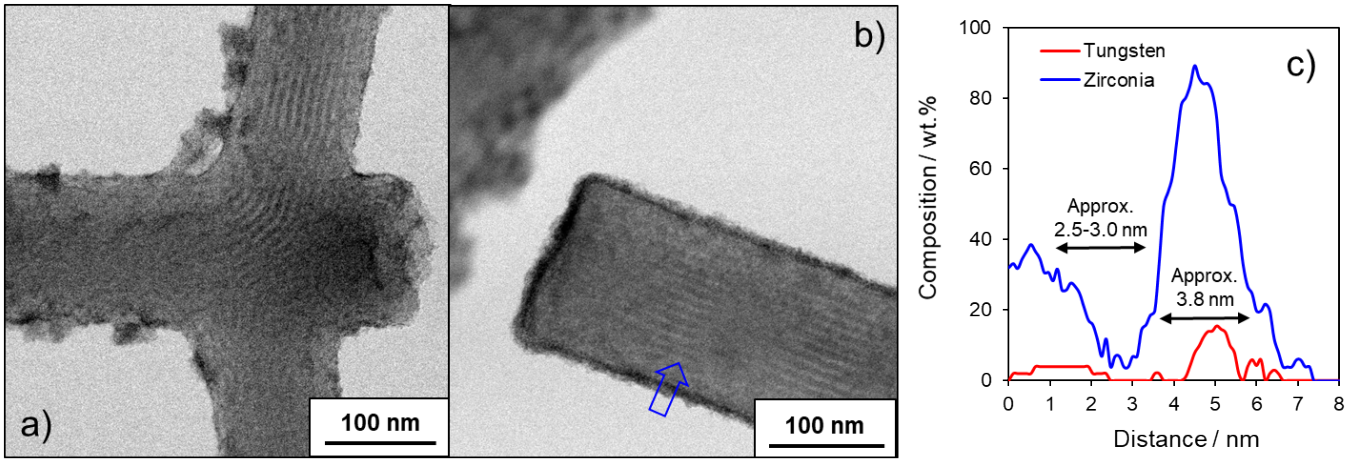

Figure S11. Representative HRTEM bright field images of WO_X/ZrOx/PMO (100%), a) and b); and c) representative elemental line scans confirming the successful co-impregnation of W and Zr species into the support mesopore network.

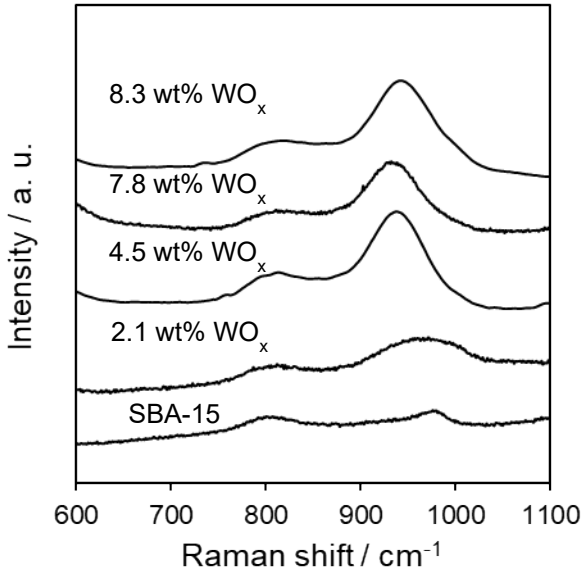

Figure S12. Loading dependant reference Raman spectra, evidencing the evolution of the WOx Raman band at ~950 cm^{-1} for WO_x/ZrO_x/SBA-15 (for indexing purposes).

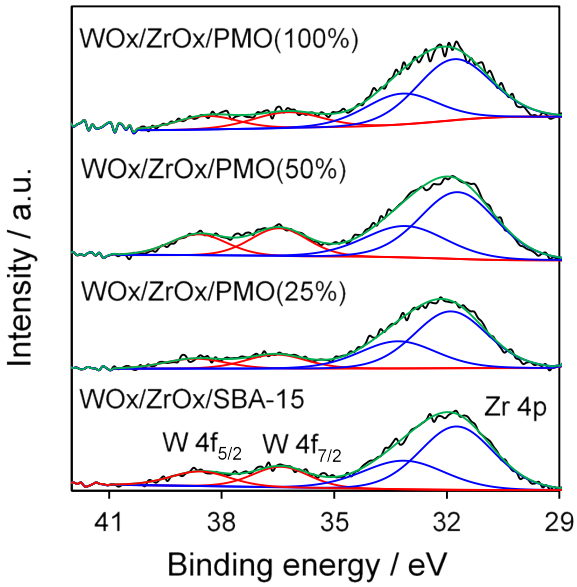

Figure S13. W 4f and Zr 4p XP spectra of WOx/ZrOx impregnated SBA-15 and PMOs.

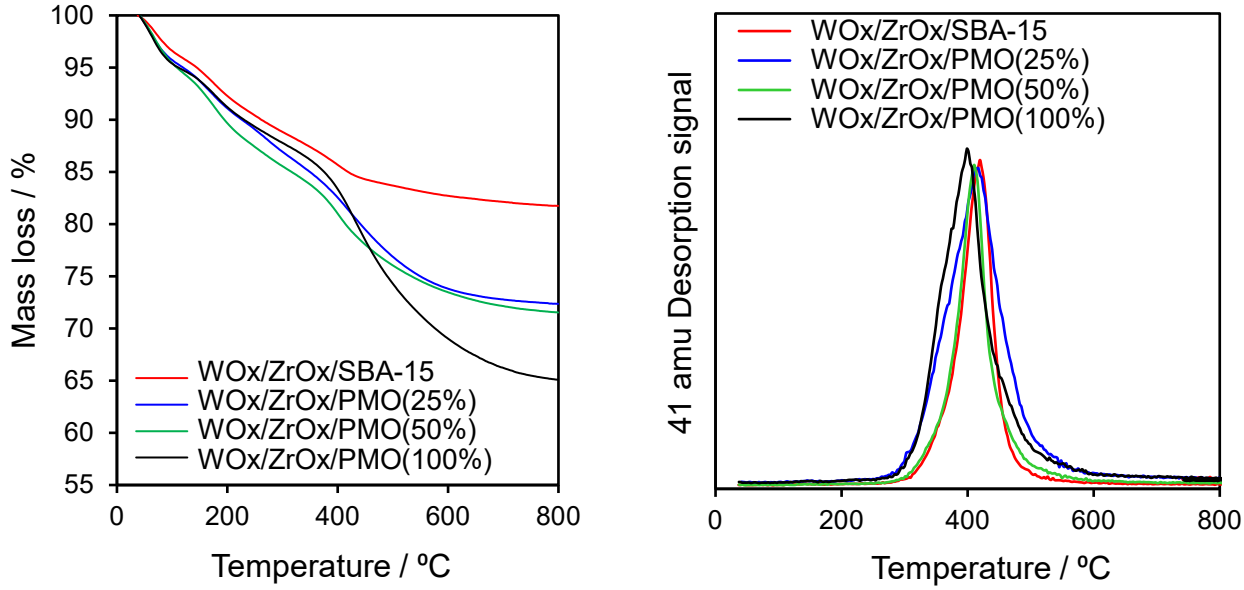

Figure S14. Thermogravimetric analysis of chemisorbed propylamine as a molecular probe of surface acidity for WOx/ZrOx impregnated SBA-15 and PMOs, (*left*) mass loss and (*right*) normalised m/z=41 amu mass spectrometer desorption signal.

Catalytic experiments

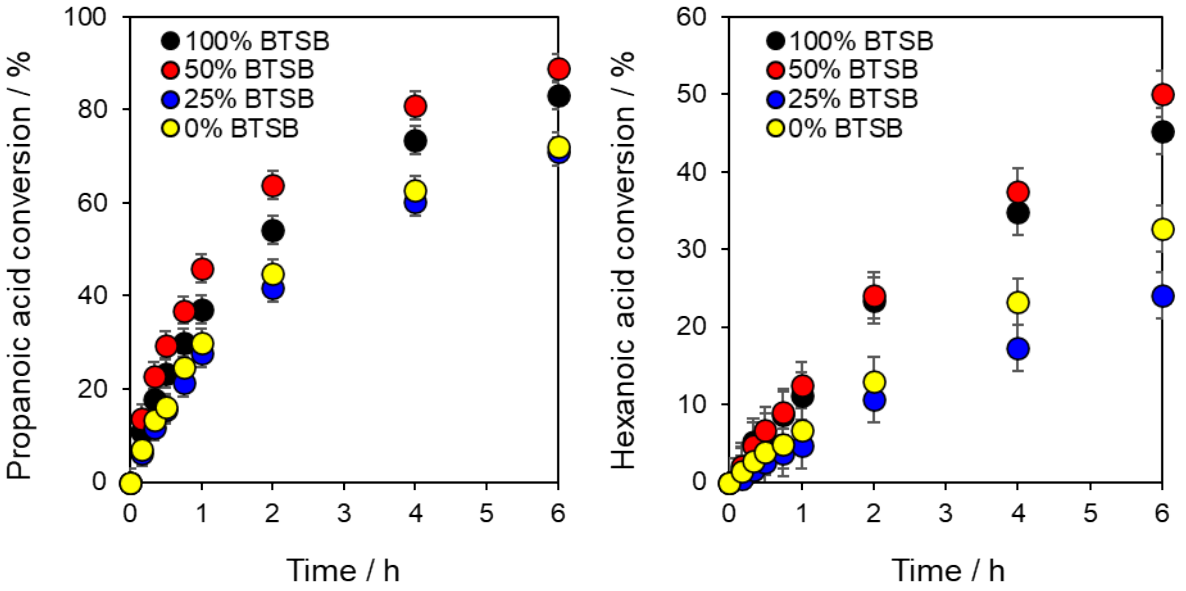

Figure S15. Reaction profiles for (*left*) propanoic acid and (*right*) hexanoic acid esterification with methanol over WOx/ZrOx impregnated SBA-15 and PMOs. Reaction conditions: 60 °C, 12.5 mL MeOH, 30:1 molar ratio MeOH: acid, 0.025 g catalyst, 800 rpm.

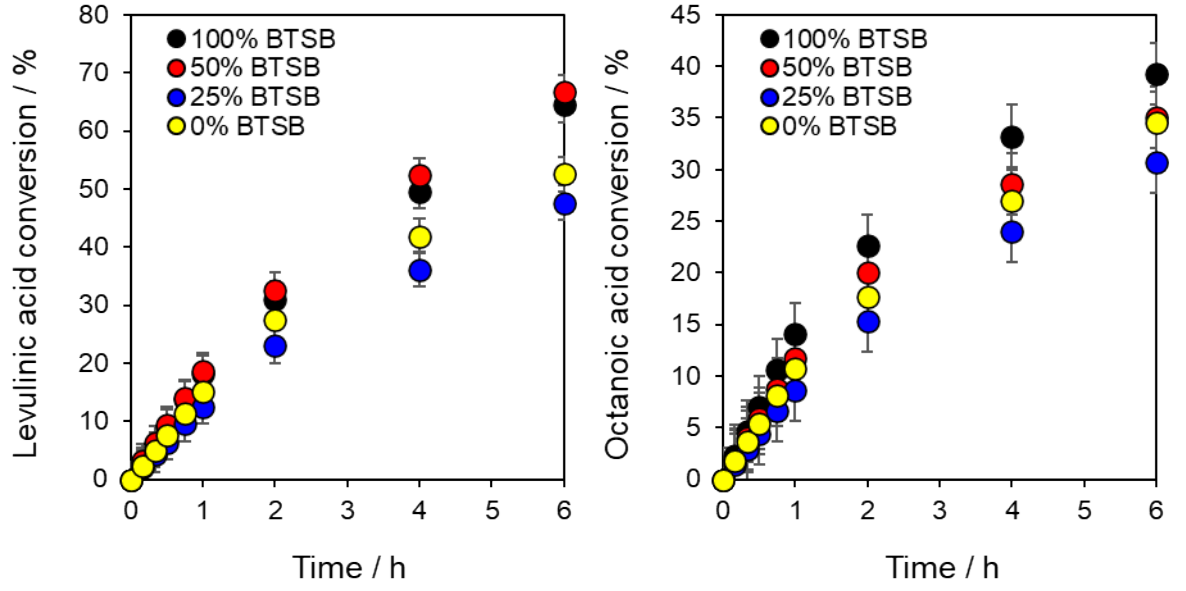

Figure S16. Reaction profiles for (*left*) levulinic acid and (*right*) octanoic acid esterification with methanol over WOx/ZrOx impregnated SBA-15 and PMOs. Reaction conditions: 60 °C, 12.5 mL MeOH, 30:1 molar ratio MeOH: acid, 0.025 g catalyst, 800 rpm.

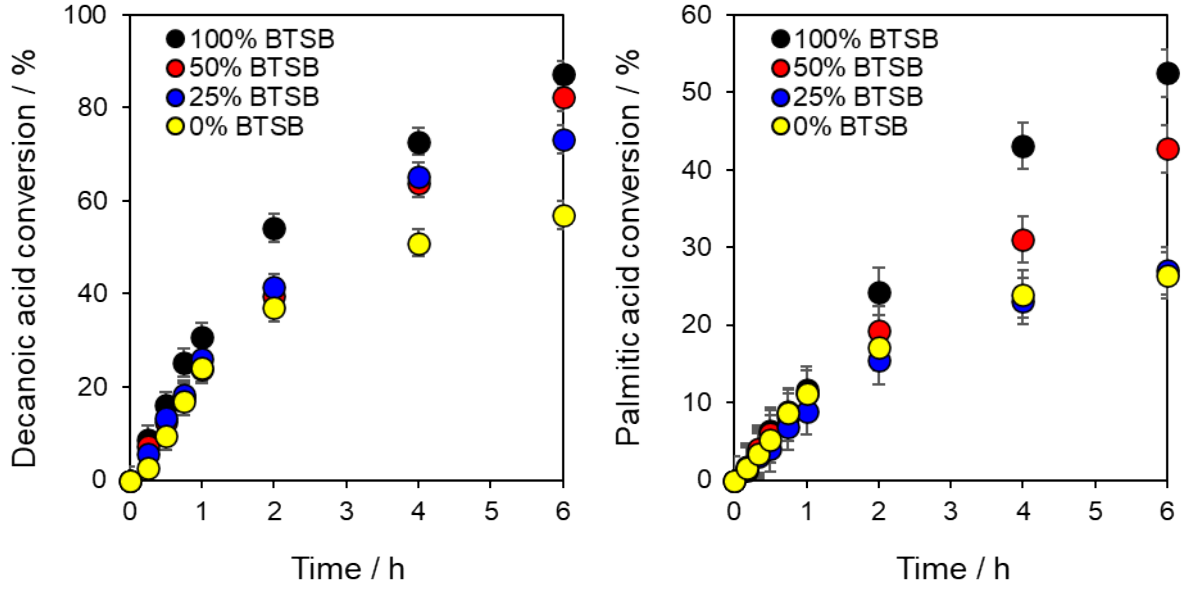

Figure S17. Reaction profiles for (*left*) decanoic acid and (*right*) palmitic acid esterification with methanol over WOx/ZrOx impregnated SBA-15 and PMOs. Reaction conditions: 60 °C, 12.5 mL MeOH, 30:1 molar ratio MeOH: acid, 0.050 g catalyst, 800 rpm.

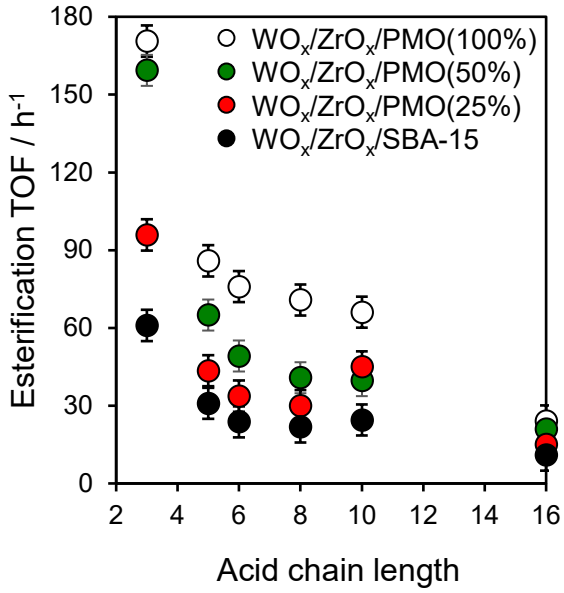

Figure S18. Turnover frequencies for C_3-C_{16} acids with methanol over WOx/ZrOx impregnated SBA-15 and PMOs. Reaction conditions: 60 °C, 12.5 mL MeOH, 30:1 molar ratio MeOH: acid, 0.025 g (C_3-C_8 acids) and 0.050 g (C_{10}–C_{16} acids) catalyst, 800 rpm.

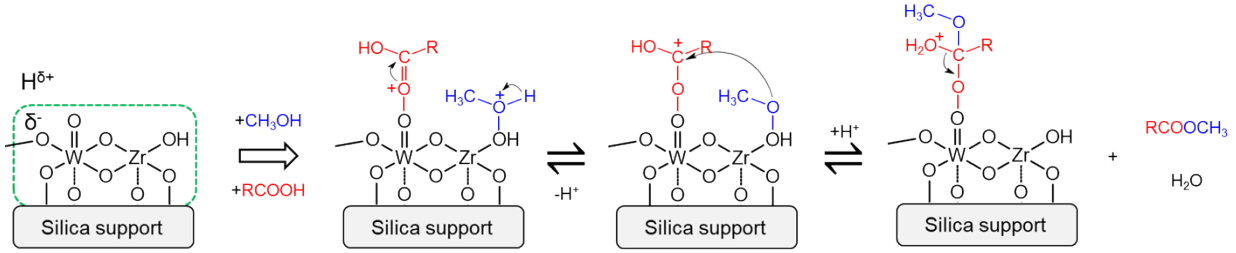

Figure S19. Proposed mechanism for carboxylic acid esterification over Lewis and Brönsted acid sites of a tungstated zirconia/silica catalyst. Adapted from ESI references 3 and 4.

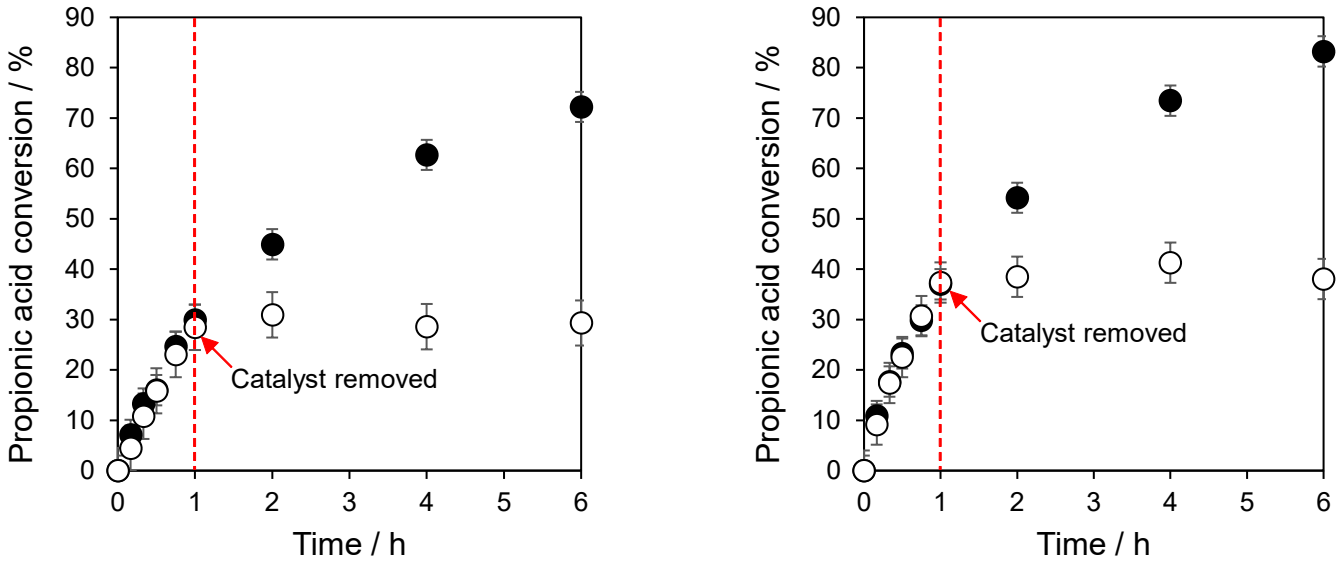

Figure S20. Hot filtration experiments for (*left*) WO_x/ZrO_2/SBA-15 and (*right*) WO_x/ZrO_x/PMO(100%) for propanoic acid with methanol esterification. Red dashed line denotes catalyst removal after 1 h. Conditions: 60 °C, 12.5 mL MeOH, 30:1 molar ratio MeOH: acid, 0.025 g catalyst, 800 rpm.

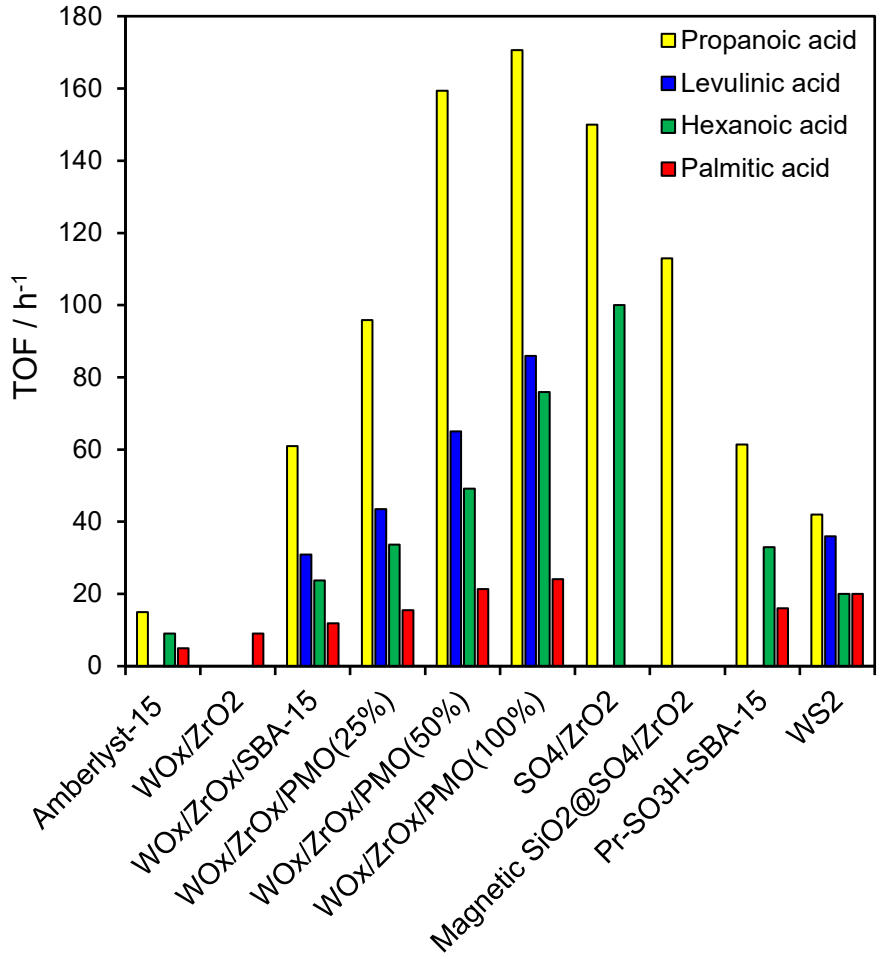

Figure S21. Solid acid catalyst performance in batchwise carboxylic acid esterification with methanol. Reaction conditions: 60 °C, 30:1 molar ratio MeOH: acid. **Catalysts:** Amberlyst-15 (this work); WOx/ZrOx/SBA-15 (this work); WOx/ZrOx/PMOs (this work); WO_x/ZrO_2;[3] SO_4/ZrO_2;[4] Magnetic $SiO_2@SO_4/ZrO_2$;[5] Pr-SO_3H/SBA-15;[6] WS_2.[7]

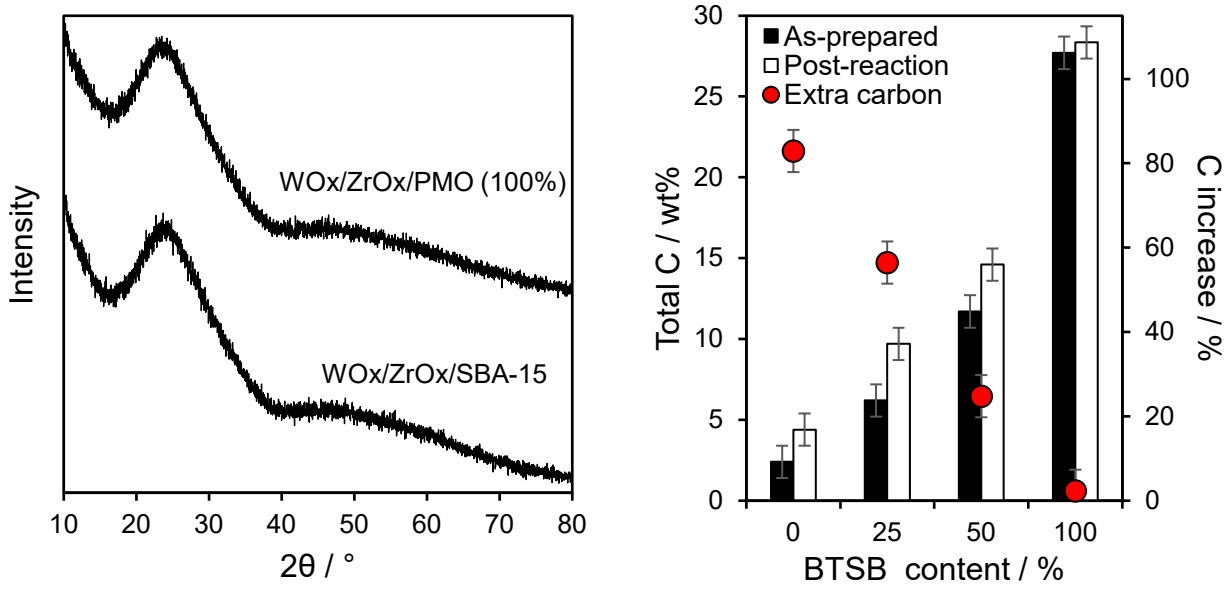

Figure S22. (*left*) Wide angle XRD patterns of WO_x/ZrO_x/SBA-15 and WO_x/ZrO_x/PMO(100%) after three propanoic acid with methanol esterification reaction cycles, and (*right*) CHN elemental analysis of as-prepared and post-reaction WO_x/ZrO_x/SBA-15 and WO_x/ZrO_x/PMOs.

Table S3. Elemental analysis (XRF) of as-prepared and post-reaction catalysts.

Catalyst	Zr / wt%	W / wt%	W:Zr mass ratio
WOx/ZrOx/SBA-15	39.4	2.1	0.05
After 3 reaction cycles WOx/ZrOx/SBA-15	37.9	2.1	0.06
WOx/ZrOx/PMO(100%)	26.3	2.0	0.07
After 3 reaction cycles WOx/ZrOx/PMO(100%)	27.2	2.1	0.08

References

(1) Sánchez-Vázquez, R.; Pirez, C.; Iglesias, J.; Wilson, K.; Lee, A. F.; Melero, J. A. Zr-Containing Hybrid Organic–Inorganic Mesoporous Materials: Hydrophobic Acid Catalysts for Biodiesel Production. *ChemCatChem* **2013**, *5* (4), 994-1001. DOI: https://doi.org/10.1002/cctc.201200527.
(2) Morales, G.; Osatiashtiani, A.; Hernández, B.; Iglesias, J.; Melero, J. A.; Paniagua, M.; Robert Brown, D.; Granollers, M.; Lee, A. F.; Wilson, K. Conformal sulfated zirconia monolayer catalysts for the one-pot synthesis of ethyl levulinate from glucose. *Chemical Communications* **2014**, *50* (79), 11742-11745, 10.1039/C4CC04594G. DOI: 10.1039/C4CC04594G.
(3) dos Santos, V. C.; Wilson, K.; Lee, A. F.; Nakagaki, S. Physicochemical properties of WOx/ZrO2 catalysts for palmitic acid esterification. *Applied Catalysis B: Environmental* **2015**, *162*, 75-84. DOI: https://doi.org/10.1016/j.apcatb.2014.06.036.
(4) Osatiashtiani, A.; Durndell, L. J.; Manayil, J. C.; Lee, A. F.; Wilson, K. Influence of alkyl chain length on sulfated zirconia catalysed batch and continuous esterification of carboxylic acids by light alcohols. *Green Chemistry* **2016**, *18* (20), 5529-5535, 10.1039/C6GC01089J. DOI: 10.1039/C6GC01089J.
(5) Tai, Z.; Isaacs, M. A.; Durndell, L. J.; Parlett, C. M. A.; Lee, A. F.; Wilson, K. Magnetically-separable Fe3O4@SiO2@SO4-ZrO2 core-shell nanoparticle catalysts for propanoic acid esterification. *Molecular Catalysis* **2018**, *449*, 137-141. DOI: https://doi.org/10.1016/j.mcat.2018.02.021.
(6) Pirez, C.; Caderon, J.-M.; Dacquin, J.-P.; Lee, A. F.; Wilson, K. Tunable KIT-6 Mesoporous Sulfonic Acid Catalysts for Fatty Acid Esterification. *ACS Catalysis* **2012**, *2* (8), 1607-1614. DOI: 10.1021/cs300161a.
(7) dos Santos, V. C.; Durndell, L. J.; Isaacs, M. A.; Parlett, C. M. A.; Wilson, K.; Lee, A. F. A new application for transition metal chalcogenides: WS_2 catalysed esterification of carboxylic acids. *Catalysis Communications* **2017**, *91*, 16-20. DOI: https://doi.org/10.1016/j.catcom.2016.12.003.